Chem. Erde **61** (2001), 117–139
Urban & Fischer Verlag
http://www.urbanfischer.de/journals/chemerd

Chemie der Erde
**Geochemistry**

# Genesis of Vein-quartz Deposits in Relation to Uplift of the Serbo-Macedonian Zone, N. Greece: Evidence from Fluid Inclusion Studies

## Genese von Gangquarzlagerstätten im Zusammenahng mit der Heraushebung der Serbo-Macedonischen Zone, N. Griechenland: Hinweise aus Flüssigkeitseinschlüssen

STEPHANOS P. KILIAS

National University of Athens, Department of Geology, Section of Economic Geology and Geochemistry, Athens, Greece

With 10 figures

Received: 18.4.2000; Accepted in revised form: 30.4.2001

## Abstract

A major group of quartz veins occur in two-mica gneisses of the polymetamorphic Vertiskos Formation (VF) of the Permian or older Serbo-Macedonian Zone. The host rocks have been affected by five metamorphic ($M_1$–$M_5$) and deformation phases ($D_1$–$D_5$). Vein emplacement in the Kastri vein-quartz deposit, Thessaloniki district, occurred along axial planes of the $D_3$ regional folding event. Vein-quartz is characterized by an early episode of ductile deformation (quartz 1), local cataclasis and dynamic recrystallization (quartz 2), overprinted by brittle fracturing. Fluid inclusion studies reveal five types of inclusions: (1) Type I, carbonic $CO_2$ ($\pm H_2O$) inclusions with calculated densities of 0.85–0.98 g/cc; (2) Type II, low salinity (0.9–14.4 wt % eq. NaCl) aqueous-carbonic $H_2O$–$CO_2$–NaCl ($\pm CH_4$–$N_2$) inclusions with highly variable aqueous:carbonic phase ratios, bubble – as well as dew-point $T_h$ between 200 and 400 °C, and a wide range of calculated densities from 0.74 to 0.99 g/cc; (3) Type III, aqueous $H_2O$-NaCl ($\pm CO_2$) inclusions ($T_h$: 130–269 °C – salinity: 2.9 to 12.7 wt % NaCl equiv. – density: 0.85–0.95 g/cc); (4) Naturally decrepitated/leaked type IV inclusions, and, (5) Type V inclusions which occupy recrystallized-unstrained quartz 2 boundaries. Types I, II, and IV occur together within quartz 1 grains either as isolated inclusions or groups, and are interpreted as coeval and most likely related to vein filling. Type III occur mainly in healed brittle fractures crosscutting both quartz 1 and 2 and are interpreted as post-vein filling hydrothermal fluids, whereas type V are very late. Natural decrepitation and leakage textures of type IV inclusions are attributed to internal overpressures, and linked to post-$D_3$ regional decompressive uplift of the VF. Uplift from mid-crustal depths is also supported by deformation microstructures in quartz which indicate that the vein was forced through the ductile-brittle transition resulting in the overprinting of ductile strain textures by brittle fractures. Wide ranges in aqueous-carbonic inclusion compositions, densities, and P-T conditions of entrapment may have been derived by a combination of various processes accompanying decompression, such as post-entrapment re-equilibration, syn- to post-metamorphic fluid evolution and immiscibility. In the absence of independent constraints on the

0009-2819/01/61/02-117 $ 15.00/0

P-T-X conditions of vein mineralization and a solid relative chronology of inclusion types I, II, and IV, a choice among alternative interpretations for variable fluid iclusion properties is difficult. However, each process may have been dependent on decompresssion and uplift. Type III late inclusions may have been trapped late along the uplift path during ongoing decompression. Uplift of VF may be related to the Late Cenozoic evolution of the region characterized by extensional tectonics.

## Zusammenfassung

Eine Gruppe von Quarzgängen kommt in einem Zwei-Glimmer-Gneis der polymetamorphen Vertiskos Formation (VF) der permischen oder älteren Serbo-Macedonischen Zone vor. Die Nebengesteine wurden von fünf metamoprhen ($M_1$–$M_5$) und fünf Deformationsphasen ($D_1$–$D_5$) beeinflußt. Die Platznahme des Ganges in der Kastri Gang-Quarz Lagerstätte im Thessaloniki Bezirk erfolgte längs axialen Ebenen des regionalen $D_3$ Faltungsereignisses. Gangquarz wird durch eine frühe Phase der duktilen Verformung (Quarz 1), lokale Kataklase und dynamische Rekristallisation (Quarz 2), überprägt von Sprödbruch, charakterisiert. Die Flüssigkeitseinschlüsse lassen sich in fünf Typen einteilen: (1) Typ I, carbonatische $CO_2$ ($\pm H_2O$)-Einschlüsse mit berechneten Dichten zwischen 0,85–0,98 g/cc; (2) Typ II, niedrig salinare (0,9–14,4 Gew.% eq. NaCl) wässrig-carbonatische $H_2O$–$CO_2$–NaCl ($\pm CH_4$–$N_2$) Einschlüsse mit stark schwankendem Verhältnis der wässrigen-carbonatischen Phasen, sowohl Blasen- als auch Taupunkt $T_h$ zwischen 200 und 400 °C und mit einem großen Bereich der der berechneten Dichten von 0,74 bis 0,99 g/cc; (3) TypIII, wässrige $H_2O$-NaCl($\pm CO_2$) Einschlüsse ($T_h$: 130–290 °C, Salinität: 2,9 bis 12,7 Gew.% eq. NaCl, Dichte: 0,85–0,95 g/cc); (4) natürlich dekripitierte bzw. ausgelaufene Typ IV-Einschlüsse, und (5) TypV-Einschlüsse, die die rekristallisierten, nicht unter Spannung stehenden Quarz 2-Genzflächen besetzen.

Typ I, II und IV kommen zusammen in Quarz 1 Körnern vor, entweder als Einzeleinschlüsse oder in Gruppen. Sie werden als gleichaltrig und in enger Beziehung zur Gangfüllung interpretiert. Typ III kommt hauptsächlich in ausgeheilten Querklüften sowohl im Quarz 1 als auch im Quarz 2 vor. Sie werden als Folge hydrothermaler Fluide nach der Gangfüllung interpretiert. Typ V Einschlüsse sind sehr spät gebildet. Natürlich dekrepitierte und ausgelaufene Gefüge von Typ IV-Einschlüssen sind verbunden mit einer internen Überpressung im Zusammenhang mit der post-$D_3$-regionalen dekompressiven Hebung von VF. Die Hebung aus mittleren Krustentiefen wird auch begründet durch Deformations-Mikrostrukturen im Quarz, welche belegen, daß die Gänge durch den duktil-spröd Übergang überprägt wurden. Erkennbar wird dies durch eine Überlagerung der duktilen Spannungstexturen von Sprödbrüchen. Die großen Zusammensetzungsschwankungen der wässrig-carbonatischen Einschlüsse, der Dichte und der P-T-Bedingungen beim Einfangen der Gase und Flüssigkeiten kann man mit einer Kombination verschiedener Prozesse, die mit der Dekompression verbunden sind, in Zusammenhang bringen. Hierbei handelt es sich um neue Gleichgewichtseinstellungen, syn- oder postmetamorphe Fluidentwicklung oder Entmischungen. Bei fehlenden Kenntnissen der P-T-X-Bedingungen während der Gangmineralisation und einer begründeten relativen Chronologie der Einschlußtypen I, II und IV ist die Entscheidung zwischen den alternativen Interpretationen für die unterschiedlichen Eigenschaften der Flüssigkeitseinschlüsse schwierig. Es steht jedoch fest, daß alle Prozesses im Zusammenhang stehen mit der Dekompression und der Heraushebung. Typ III Einschlüsse entstanden später während des Hebungsprozesses bei fortschreitender Dekompression.Die Hebung von VF kann mit der spät-känozoischen Entwicklung im Zusammenhang mit einer Dehnungstektonik in Verbindung gebracht werden.

## Introduction

Significant reserves of vein-quartz amounting to about 2.5 m.t occur in two-mica gneisses of the Vertiskos Formation (VF) of the Serbo-Macedonian Zone (SMZ) in N. Greece (ARVANITIDIS and KILIAS, 1997). The veins share broad similarities in nature and

occurrence. Most quartz veins cluster in the northwestern part of SMZ, fill NNW-SSE trending structures, conform to or crosscut the main schistosity of the host gneisses, are deformed in a transitional ductile-brittle rheological regime and, share common fluid inclusion characteristics (ARVANITIDIS and KILIAS, 1997). Fluid inclusion studies of quartz veins were undertaken for the implementation of a European Commission-funded Program entitled "New industrial applications for quartz deposits indigenous to the Community", which evaluated the purity of Greek vein-quartz for high-tech industrial applications (ARVANITIDIS, 1998).

The present fluid inclusion study concentrates on the Kastri vein-quartz deposit that is exploited by The Hellenic Industrial Minerals SA (in Greece known as ELVIOR), in the Kastri area some 30 km northeast of Thessaloniki (Fig. 1). Recoverable reserves of quartz amount to 100,000 metric tones. The Kastri quarry produces vein-quartz that after processing is used in the glass and ceramics industries. This paper gives petrographic and microthermometric results and genetic interpretations arising from a fluid inclusion study of vein-quartz from the Kastri deposit and further discusses the significance of the genetic interpretation in the regional geologic evolution of Vertiskos Formation.

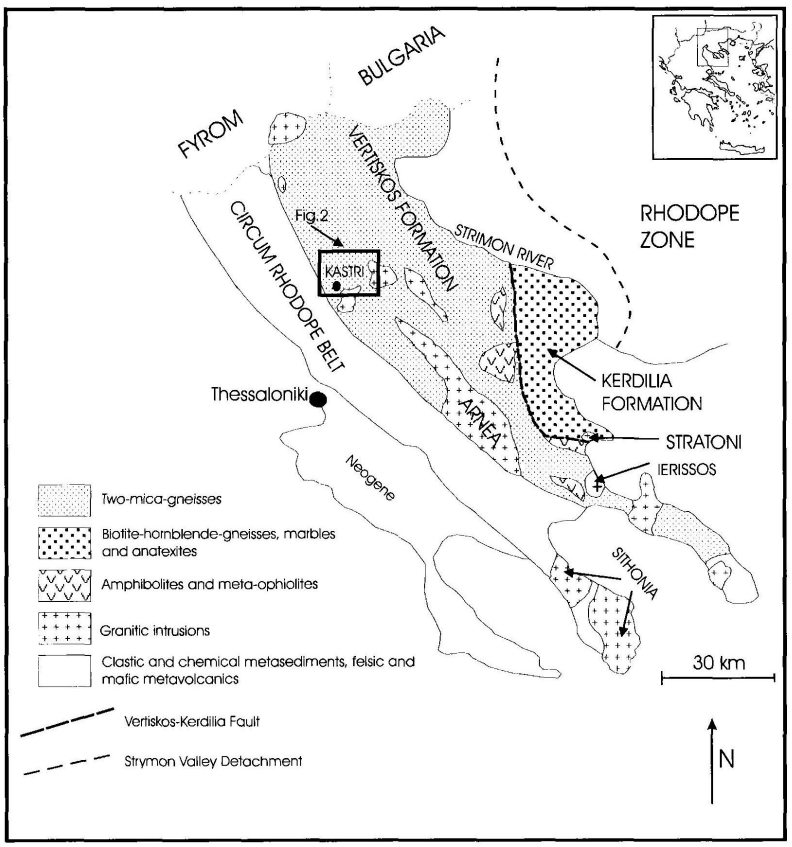


**Fig. 1.** Geotectonic map of the Serbo-Macedonian Zone (modified after KOCKEL et al., 1977)

## Regional geologic setting

The Serbo-Macedonian Zone (SMZ) is a narrow NW-SE trending heterogeneous ophiolite-bearing high-grade metamorphic terrain that is bounded against the Rhodope Zone (RZ) to the east by the Strimon Valley Fault, a west dipping Neogene extensional detachment (Strimon Valley detachment) (DINTER and ROYDEN, 1993; DINTER 1998), and by underthrusted Permian-Mesozoic meta-sediments of the Circum-Rhodope Belt (CRB) on the west (KAUFMANN et al., 1976) (Fig. 1). Studies of the tectonometamorphic evolution of the SMZ have revealed a very complex succession of metamorphic, and deformation, episodes which possibly represent parts of more than one orogenic cycles (PATRAS et al., 1986; SAKELLARIOU, 1989; DIMITRIADIS and GODELITSAS, 1991; SIDIROPOULOS, 1991; KOUROU, 1991). It is generally agreed that the SMZ and RZ have a common origin, and represent either Eurasian continental margin in the Permian which has not been significantly displaced from its site of origin or, an accretionary wedge assembled from Permian or older continental, and oceanic (Tethyan), rocks (MOUNTRAKIS, 1994). Both the Serbo-Macedonian and Rhodope Zones were incorporated in a Late Jurassic-Cretaceous marginal orogen during Alpine convergence between Africa and Europe, and metamorphosed under high-P-high-T conditions (MOUNTRAKIS, 1994; DINTER, 1998). However, evidence for earlier Hercynian and pre-Hercynian metamorphic episodes has been found locally in the SMZ (SAKELLARIOU, 1989; DIMITRIADIS and GODELITSAS, 1991; SIDIROPOULOS, 1991; KOUROU, 1991). During Late Cenozoic extensional dismemberment of the Alpine collisional orogen, the SMZ was translated southwestward to its present location in the hanging wall of the Strimon Valley detachment from a former position overlying the southwestern RZ (DINTER, 1998) (Fig. 1). The SMZ was divided by KOCKEL et al. (1977) into two units, the Vertiskos Formation (VF) in the west and the underlying Kerdilia Formation (KF) in the east (Fig. 1). The two formations are separated by the highly mineralized west-dipping Vertiskos-Kerdilia normal fault, that was interpreted by DINTER (1998) as coeval and synthetic to the Strymon Valley detachment (Fig. 1). Both formations are intruded by Mesozoic (i.e. Arnea) and/or Tertiary (i.e. Sithonia, Ierissos, Stratoni) granitic bodies and porphyries (FREI, 1992; CHRISTOFIDES et al., 1990; DE WET et al., 1989; VITAL, 1986) (Fig. 1).

## Local geology

The Kastri region consists of rocks belonging to the NW part of the Vertiskos Formation, and to a lesser extent by rocks of the Permo-Triassic Examili Formation (EF) (KOCKEL et al., 1977; KOUGOULIS et al., 1990) belonging to the Circum-Rhodope Belt. The NW part of the VF consists of meta-sedimentary two-mica gneisses, semi-pelitic and psammitic schists, meta-tholeiitic eclogite and amphibolite bodies, serpentinized ultramafics, anatectic granites, and pegmatites (KOCKEL et al., 1977; KOUROU, 1991; SIDIROPOULOS, 1991). The Examili Formation in the area is represented by clastic meta-sediments and acid meta-volcanics (Fig. 2).

Five metamorphic episodes ($M_1$–$M_5$) and four major deformation phases ($D_1$–$D_4$) have been recognized in the northwestern part of Vertiskos Formation (KOUROU, 1991; SIDIROPOULOS, 1991). The rocks have suffered Alpidic (Late Jurassic) deformation ($D_3$) and regional metamorphism ($M_4$), which reached upper greenschist-facies conditions

(T: 440–520 °C, P = 5–6 or 9 kbar). The $M_4$ metamorphic event has been interpreted as a result of static heating of the system. According to other workers in the central and southern parts of VF, Alpine (Late Jurassic to Early Cretaceous) metamorphism reached a peak of amphibolite-facies conditions (PATRAS et al., 1986; SAKELLARIOU, 1989). Synchronous to the $M_4$–$D_3$ event is the intrusion of the Polydendri anatectic granite (KOUROU, 1991) (Fig. 2). Contact metamorphic phenomena have not been observed (KOUROU, 1991). The $M_4$–$D_3$ tectono-metamorphic event was followed by a post-Jurassic $D_4$ deformation phase and retrogression under greenschist facies ($M_5$) (T: 300–500 °C, P = < 5 kbar). This greenschist facies retrogressive overprint may have lasted until Eocene/Oligocene (HARRE et al., 1968; ECHTLER et al., 1987) and marked the end of Alpine metamorphism. $D_3$ deformation is characterized by tight to isoclinal shear folds,

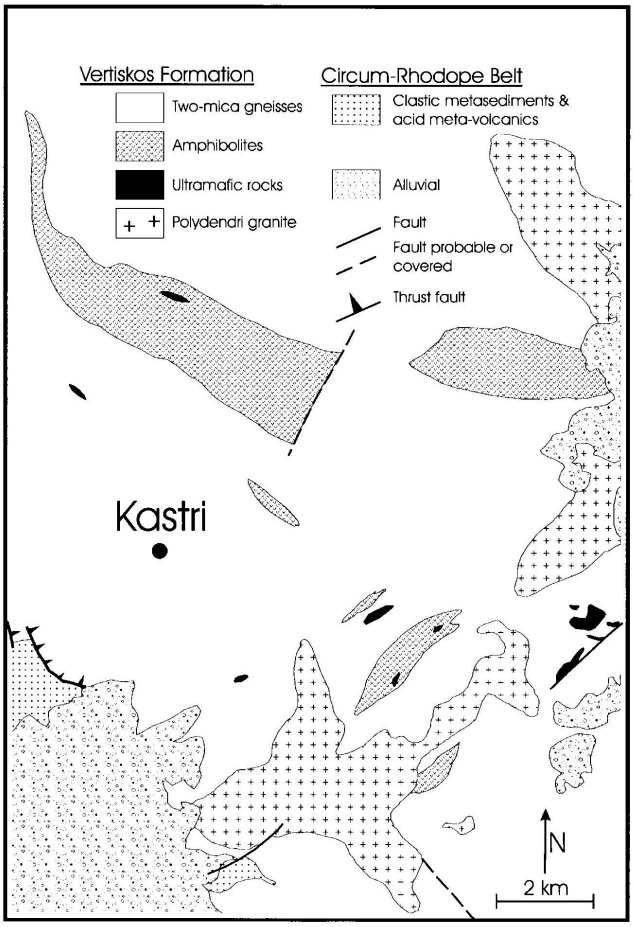


**Fig. 2.** Geologic map of the Kastri region (KOCKEL et al., 1977; VERANIS et al., 1990) (IGME map 1:50.000 LACHANAS sheet).

and produced the prominent regional $S_3$ axial plane schistosity, whereas $D_4$ has open folds oriented NNW-SSE to NNE-SSW. Post-$D_4$ deformation ($D_5$) was characterized by extensional brittle phenomena (KOUROU, 1991; SIDIROPOULOS, 1991). Evidence for Hercynian (?) (Amphibolite Facies – $M_2$–$M_3$–$D_2$) and Pre-Hercynian (Eclogite facies – $M_1$–$D_1$) tectonic and/or metamorphic events exist locally. The rocks of Examili Formation have been metamorphosed to greenschist facies metamorphism (VERANIS et al., 1990).

A Late Alpine or post-Alpine age is suggested for quartz veins in the northern part of VF as they either conform to (strike NNW-SSE, dip 90°–40°) or cut (strike NE-SW to E-W, rarely with vertical dip) the regional Late Alpine $S_3$ schistosity.

## Kastri deposit

The deposit is hosted in two-mica gneisses and biotite gneisses, and forms disrupted steeply-dipping vein-bodies and discontinuous lenses which are concordant to the regional 340-striking schistosity $S_3$ (Fig. 3). Although the vein-bodies and lenses show some signs of tectonic disturbance (see below), evidence of the $D_1$–$D_2$ deformation is lacking. Field relations suggest that vein emplacement occurred along axial planes of the

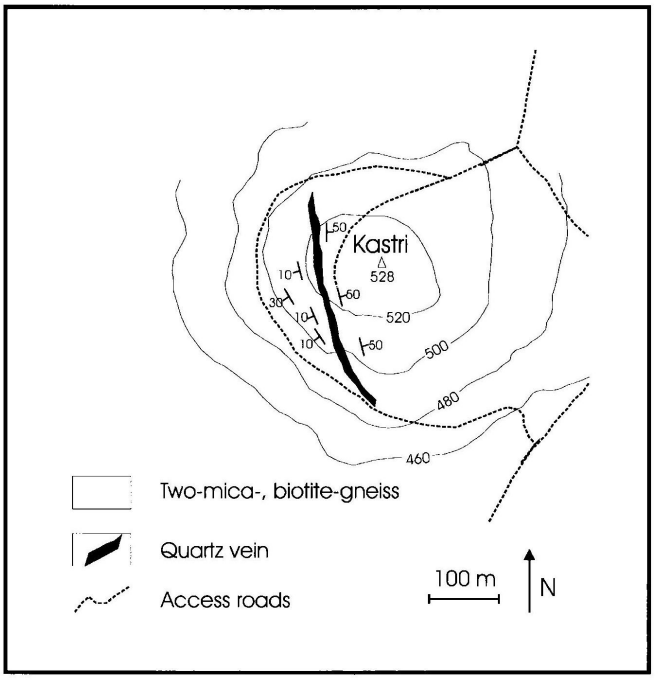


**Fig. 3.** Geological map of the Kastri quartz vein (N. VERANIS – IGME, unpubl. data).

$D_3$ folding event. The contact between the veins and the host rocks is abrupt without alteration. The deposit is 350m in lateral extent and individual quartz bodies or lenses are 5–13 m wide.

The Kastri quartz vein is composed chiefly of milky or yellowish-brown quartz (up to 99.5% by volume) with local traces of chlorite and iron oxides. Vein quartz is deformed and comprises subhedral to anhedral elongated grains, which are slightly oriented along their longest axis. Quartz grain dimensions are up to 8 mm in their longest axis and up to 4 mm in width.

Vein quartz has undergone an early episode of syn-depositional ductile deformation (quartz 1) (Fig. 4A, B). Such deformation may be attributed to emplacement of veins in a dynamic tectonic environment. Ductile deformation was followed by local cataclasis and recrystallization (quartz 2) (Fig. 4C), and superimposed extensive brittle fracturing. Brittle fractures crosscut quartz 1 and 2, and are marked by trails of aqueous fluid inclusions (see below) which record the sealing and healing of brittle microcracks by hydrothermal fluids (Fig. 4D, 4E).

## Fluid inclusions

### Sampling and laboratory procedure

Fifteen (15) samples of seven quartz bodies covering a horizontal interval of about 350 m within the Kastri quarry were collected for fluid inclusion microthermometric studies. Microthermometry was conducted on a LINKAM THMS600/TP92 heating/freezing system calibrated with natural pure $CO_2$ inclusions, pure $H_2O$ and various organic solvents. The accuracy of the measurements (multiple measurements of the same inclusion) was determined to be better than ±0.5 °C over the temperature range of –70 °C to +30 °C and ± 2–3 °C for temperatures up to 450 °C.

### Types and occurrence of fluid inclusions

Five types of fluid inclusions were identified:

**Type I inclusions:** These fluid inclusions, at room temperature, are one-phase $CO_2$-dominated liquid inclusions, which nucleate a $CO_2$-rich vapor bubble on cooling to 20 °C. No aqueous phase was seen in any type I inclusions but may have been present as a thin film wetting the inclusion walls. Type I inclusions represent <10% of all inclusions. They occur mostly as isolated inclusions and have elliptical, angular to subrounded shape. Top widths of type I inclusions were measured to be <5 to 12 μm.

**Type II inclusions:** At room temperature these inclusions are characterized by visible amounts of both aqueous liquid plus $CO_2$ and consist either of three phases (liquid water+liquid $CO_2$ + $CO_2$-rich vapor) or two phases (liquid water + $CO_2$-rich liquid/vapor). The volumetric percentage of the $CO_2$-rich (liquid + vapor) phase at room temperature ranges from 10 to 90%. Most inclusions fall either in the range between 10 and 40 vol.% $CO_2$ or 70 and 90 vol.% $CO_2$. Type II inclusions have two types of occurrence. First, as isolated inclusions with subrounded or rectangular shapes (Fig. 5B) and secondly, as low density inclusion irregular clusters consisting of rectangular or elliptical inclusions. Top widths of type II inclusions were measured to be <5 to 15 μm.

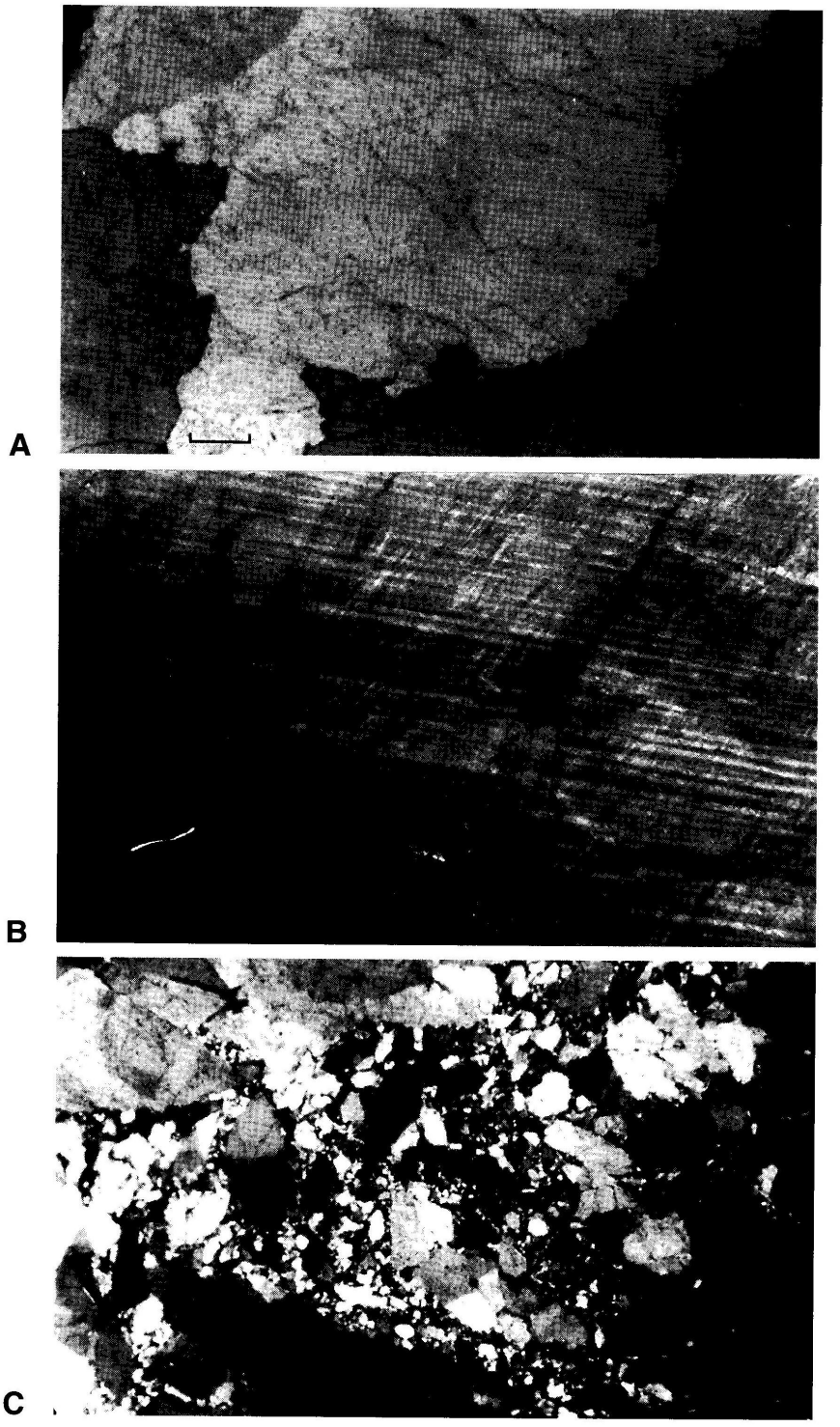
A
B
C

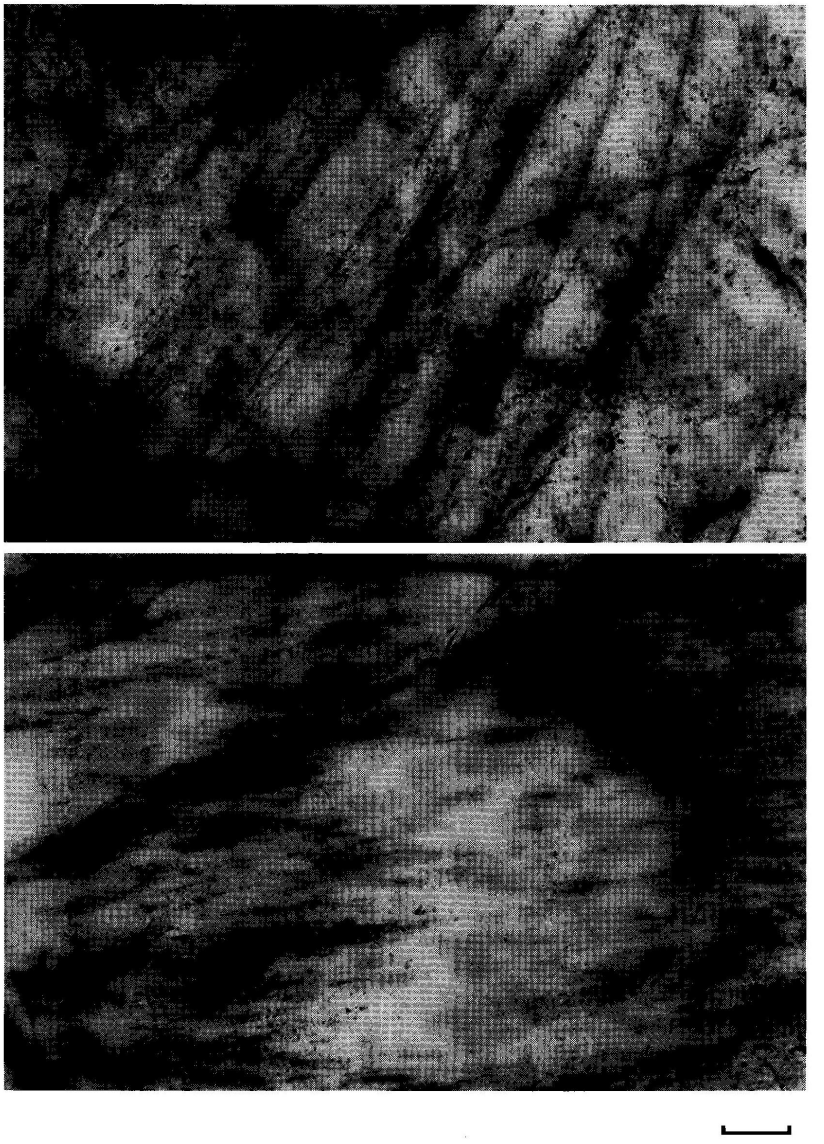


**Fig. 4.** Deformation microstructures in vein-quartz. **A–C:** Bar ≙ 250 μm; **D+E:** Bar ≙ 100 μm. **A.** Relatively unstrained substrate of coarse anhedral quartz grains with homogeneous to slight undulose extinction, and curved to embayed boundaries (quartz 1). Primary quartz with superimposed ductile strain and subsequent brittle fracturing. **B.** Translation gliding expressed as fine deformation lamellae. **C.** Cataclastic Texture. Large old strained grains surrounded by fine, recrystallized new quartz (2). **D.** Dense network of subparallel closely spaced quasilinear to curved secondary fluid inclusion trails along healed microfractures. At least two fracture sets can be seen. **E.** Intragranular secondary fluid inclusion trails delineating healed microfractures affecting matrix quartz.

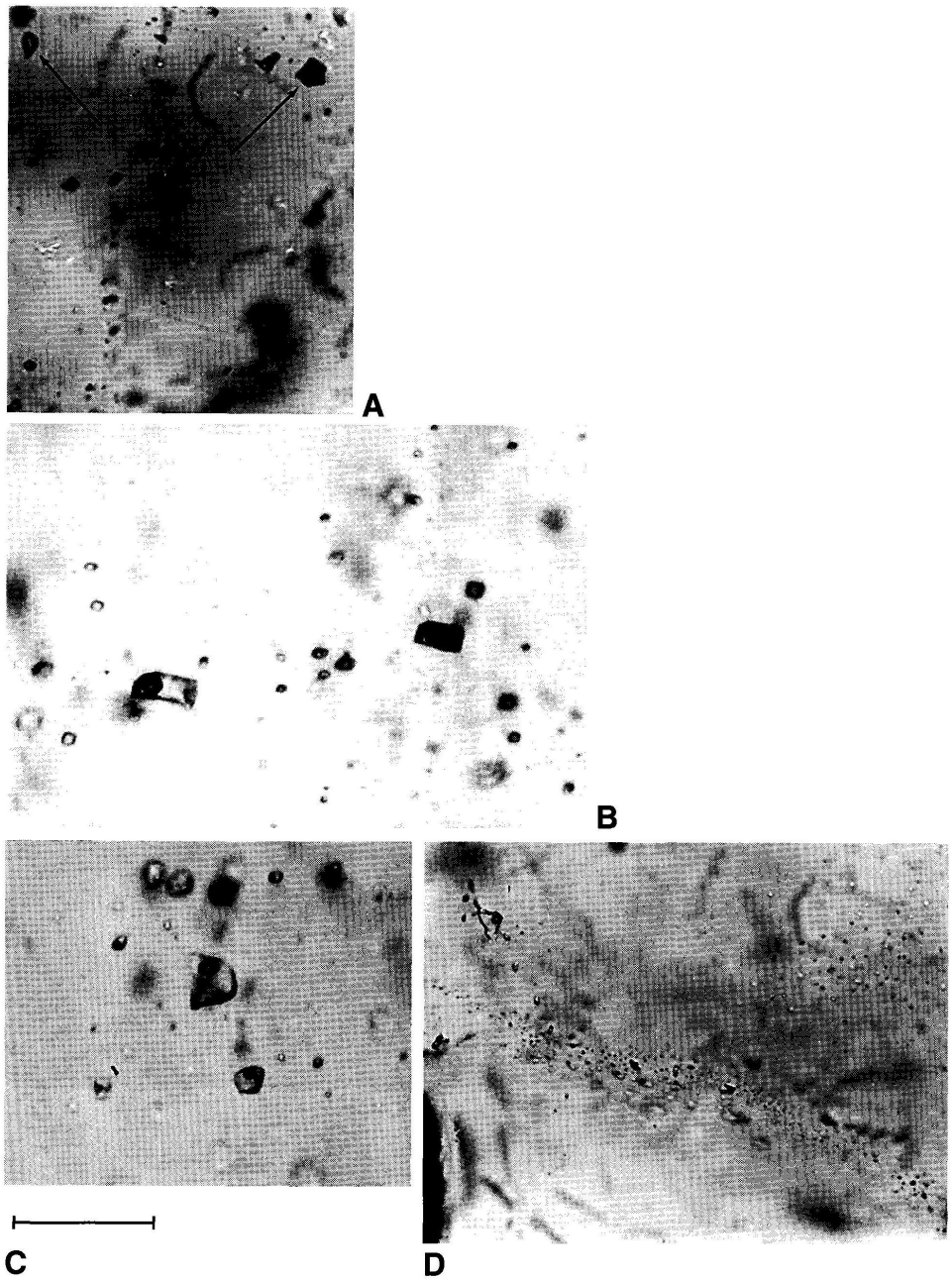


**Fig. 5.** Fluid inclusion types in vein-quartz. Bar ≙ 50 μm
**A.** Dark type IV leaked inclusions in quartzn 1(arrows). **B.** Coexisting $H_2O$-rich and $CO_2$-rich type II inclusions in quartz 1. **C.** Type III liquid-vapor inclusions in quartz 1. **D.** Healed fracture containing secondary type III inclusions.

**Type III inclusions:** These fluid inclusions consist of two ($H_2O$-rich liquid + vapor) or one (liquid water) phase at room temperature (Fig. 5C). The vapor phase occupies 10–20% of the inclusion volume. They occur mainly as trails along secondary intragranular or transgranular healed fractures (Fig. 4D, 4E, 5D) and their coexistence with the other types in random clusters is very limited. Their shape varies from angular to subrounded. On the basis of clathrate melting phenomena some random type III inclusions may contain a very small amount of dissolved $CO_2$ (see below). Type III inclusions have top widths of <5 to 20 μm.

**Type IV** represent naturally decrepitated or re-equilibrated inclusions. The term "re-equilibration" is used here to include any obvious changes in the inclusion density and/or texture (e.g. VITYK et al., 1995; 1996). Sizes range from 10 (leaked variety) (Fig. 5A) to 200 μm (decrepitated variety) in the longest dimension (Fig. 6B, C) They all lie well within quartz crystals either irregularly distributed or in intragranular healed fractures (Fig. 5A; 6B, C). Decrepitated type IV inclusions are either empty or refilled with a younger fluid, or contain a vapor phase. They have highly irregular shapes with rough outlines, and are commonly surrounded by planar halos of small irregular to rounded satellite inclusions (<5 μm) with inconsistent vapor/liquid ratios (Fig. 6B, C). Dark inclusions as a result of high internal reflections (either isolated, or in other inclusion clusters or trails) that do not nucleate a vapor phase on cooling (Fig. 5A) have been interpreted as leaked empty inclusions or only to contain a vapor phase. These inclusions lack the usual morphologies of decrepitated inclusions and tend to have negative crystal, regular oval, or angular to rounded shapes (Fig. 5A).

**Type V** inclusions occupy recrystallized-unstrained grain (quartz 2) boundaries. Some of them are worm shaped, irregular voids and dentritical channels (Fig. 6A), which are typical of grain boundaries (BAKKER and MAMTANI, 2000).

### Possible relative timing of fluid inclusions

Given their mode of occurrence, inclusion types I, II, IV are interpreted as most likely related to vein filling, whereas type III inclusions are related to post vein filling hydrothermal processes related to late brittle deformation. Type IV inclusions may represent inclusions trapped in the early stages of vein growth, and possibly synchronous with $D_3$ or $D_4$ deformation, which experienced destructive decrepitation after entrapment. Type I and II inclusions are spatially associated with type IV inclusions in quartz 1, and thus they may belong to the same generation with type IV. Unambiguous later post-$D_4$ origin has been assigned to fracture controlled type III inclusions which crosscut both quartz 1 and 2 (Fig. 6A). Moreover, based on the lack of systematic differences in microthermometry data (see below) it is indicated that random and fracture controlled type III inclusions are coeval. Therefore, all type III inclusions have been interpreted as post dating types I, II and IV. Type V inclusions are extremely late and of minor importance in as much that they are still open to any fluid system that may flow along grain boundaries.

## Microthermometry results

Recently designed computer programs FLUIDS (BAKKER, 1999a), GASWET (BAKKER, 1999b), and CLATHRATES (BAKKER, 1997) were used for the interpretation

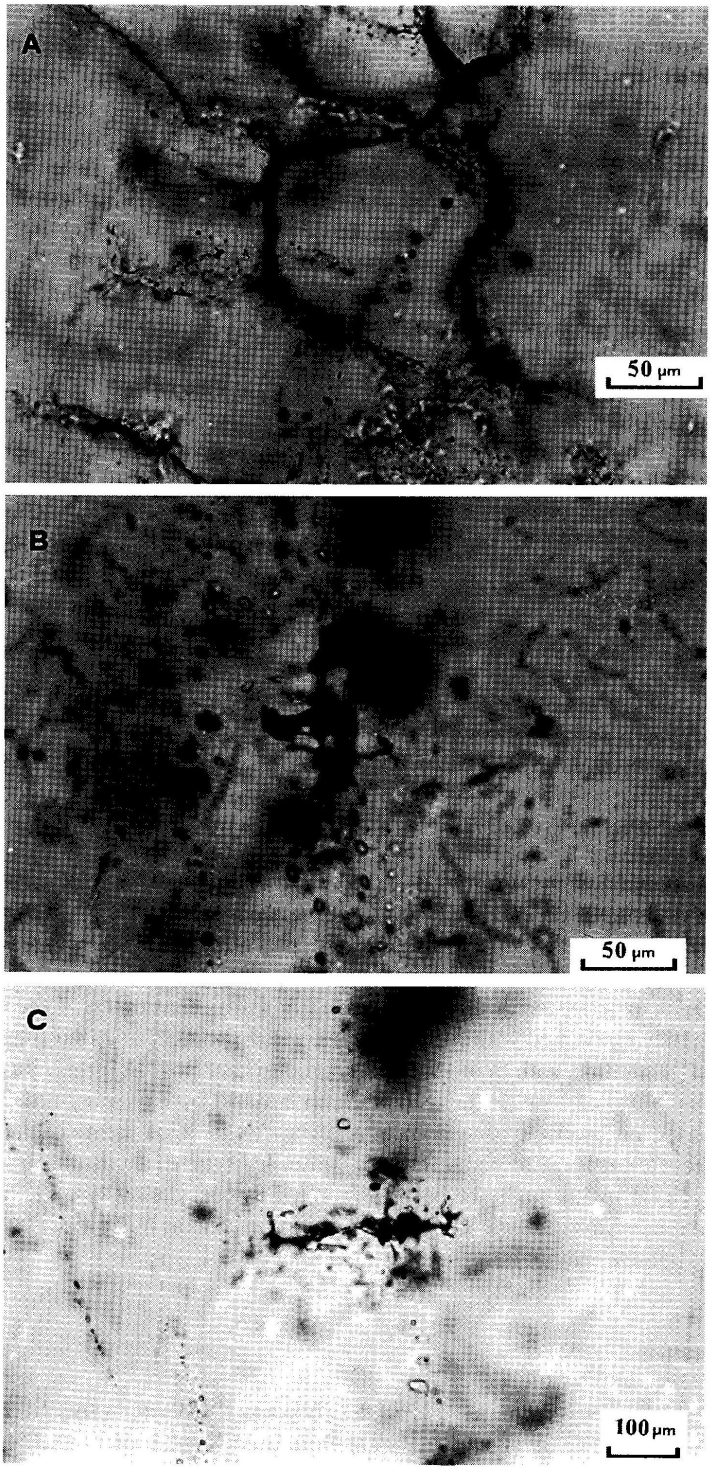
A
50 μm
B
50 μm
C
100 μm

of microthermometry data in order to calculate fluid inclusion compositions and densities. Recently published equations of state are incorporated in these programs.

**Type I inclusions:** Final melting temperatures of solid $CO_2$ ($TmCO_2$) in type I inclusions range narrowly from –57 to –56.7 °C (Fig. 7A) indicating that the carbonic phase of type I inclusions is nearly pure $CO_2$. Therefore, type I inclusions were interpreted in the pure $CO_2$ fluid system. Homogenization temperatures of the carbonic phase range widely from –11.0 to +10.6 °C (Fig. 7B). Homogenization of the carbonic phase always occurred to the liquid phase. Microthermometric data correspond to densities ranging between 0.85 and 0.98 g/cc. Volumetric properties of type I inclusions were calculated in the pure $CO_2$ fluid system with the use of equations of state (EOS) from DUSCHEK et al. (1990) and SPAN and WAGNER (1996) (see BAKKER, 1997).

**Type II inclusions:** Final melting temperatures of solid $CO_2$ ($TmCO_2$) in type II inclusions were between –60.9 to –56.9 °C (mode at –57.7 °C) (Fig. 7C). These data indicate the presence of gas other than $CO_2$ in the carbonic phase in some inclusions. In the absence of Raman analysis, and in order to estimate V-X fluid properties of the carbonic phase mixture in type II inclusions, it was assumed that the observed depression of $TmCO_2$ below that of pure $CO_2$ reflected the influence of only one other gas species, either $CH_4$ or $N_2$. The liquid and vapor phases of the carbonic phase homogenized to the liquid between +4.0 and +29.9 °C (Fig. 7D). The composition of the carbonic phase, estimated graphically using the V-X diagrams for the binary systems $CO_2$–$CH_4$ and $CO_2$–$N_2$ from THIERY et al. (1994), vary between approximately 86 and 99 mole % $CO_2$. Interpreted in terms of binary $CO_2$–$CH_4$ or $CO_2$–$N_2$ compositions, calculated densities of the carbonic phase mixture vary between 0.60 and 0.90 g/cc. Liquid-vapor equilibria of carbonic $CO_2$(–$CH_4$–$N_2$) mixtures in type II inclusions (i.e. conversion of homogenization temperatures into densities at bubble-points) were calculated by using the modified

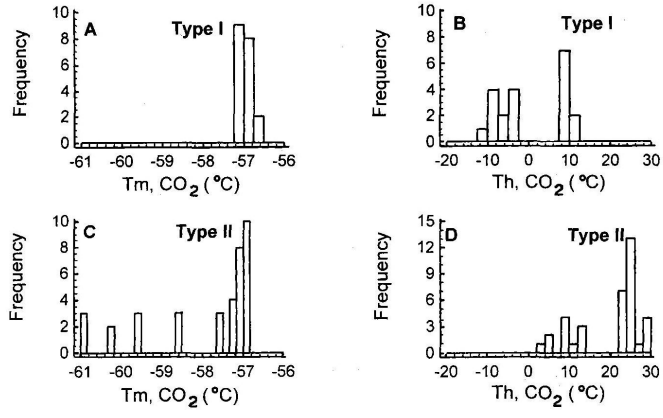


**Fig. 7. A.** Histogram of solid $CO_2$ melting temperatures (Tm, $CO_2$) of type I inclusions. **B.** Histogram of $CO_2$-phase homogenization temperatures (Th, $CO_2$) of type I inclusions. **C.** Histogram of solid $CO_2$ melting temperatures (Tm, $CO_2$) of type II inclusions. **D.** Histogram of $CO_2$-phase homogenization temperatures (Th, $CO_2$) of type II inclusions.

◄

**Fig. 6.** Fluid inclusion types in vein-quartz.
**A.** Type V inclusions at grain boundaries of recrystallized quartz 2. Note healed fracture delineated by type III inclusions, transecting central quartz sub-grain. **B.** Large type IV decrepitated inclusion (center). **C.** Decrepitated type IV inclusions surrounded by halos of small irregular to rounded satellite inclusions.

Soave equation of state according to THIERY et al. (1994) using LEE and KESLER (1975) for volumetric properties (see BAKKER, 1997).

Temperatures of final clathrate melting (Tm, clath) in the presence of both liquid and vapor $CO_2$ ($\pm CH_4$) range from +1.7 to +11.0 °C (Fig. 8A). Interpreted in terms of $H_2O$–NaCl–$CO_2$ (–$CH_4$ or –$N_2$) compositions, Tm,clath (below +10.1 °C) corresponds to salinities ranging from 0.9 to 14.4 wt% eq NaCl. Salinity of type II inclusions was calculated from clathrate melting temperatures (Fig. 8A) at $Q_2$ conditions by using purely empirical equations from DARLING (1991), DIAMOND (1992) and BAKKER et al. (1996) (see BAKKER, 1997). The few clathrate melting temperatures higher than +10.1 °C are also attributed to the presence of other gases ($CH_4$ or $N_2$) in addition to $CO_2$.

Total homogenization temperatures vary between 199° and 403 °C (Fig. 8B, C). Homogenization occurred to both the carbonic and the aqueous phases in the range 200° to 403 °C (average value 292 °C) (Fig. 8B) and 199° to 371 °C (average value 265 °C) (Fig. 8C), respectively. Homogenization temperature frequency histograms are flat, skewed to high temperatures, and show high ranges and high standard deviation (292 ± 65 °C and 265 ± 52 °C) (Fig. 8B, C). Some type II inclusions decrepitated before homogenization (estimated visually) at temperatures ranging from 200° to 390 °C. These temperatures were used as minimum homogenization temperatures. Calculated bulk densities for type II inclusions in the system $H_2O$-$CO_2$-NaCl-$CH_4$(or –$N_2$) range from 0.74 to 0.99 g/cc. Assuming a ±10 % error inherent in the estimation of volume fractions of the fluid phases, the calculated densities may vary by approximately ± 0.02–0.04 g/cc. Bulk densities were calculated with the use of computer program Q2 of CLATHRATES.

**Type III inclusions:** No systematic differences of microthermometric properties were observed between random and fracture controlled type III inclusions. Therefore, data are treated collectively. Temperatures of first ice melting (eutectic temperature) were recorded between –22° and –37.1 °C suggesting the presence of dissolved KCl/$MgCl_2$ in addition to NaCl (BORISENKO, 1977 in SHEPHERD et al., 1985). Final ice melting (Tm, ice) of type III inclusions were recorded at temperatures between –2.2 and –8.9 °C indicating salinities between 2.9 and 12.7 wt% eq. NaCl (Fig. 9A). Salinities were interpreted in the system $H_2O$-NaCl on the basis of BODNAR (1993). A few clathrate melting temperatures were recorded for some random type III inclusions in the range between +3.5 and +8.9 °C and were interpreted in terms of low (up to 2.2 molal) $CO_2$ contents in these type III

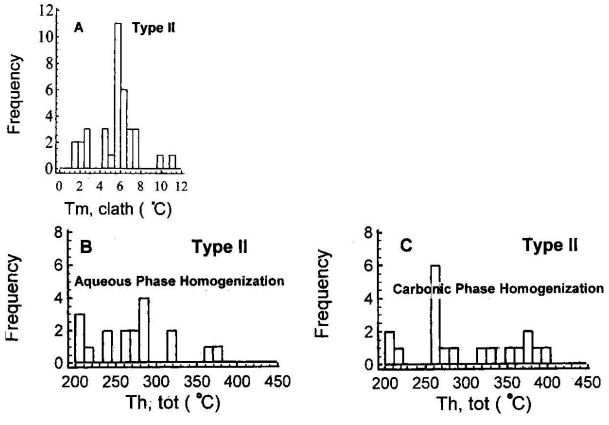


**Fig. 8. A.** Histogram of clathrate melting temperatures (Tm, clath) of type II inclusions. **B, C.** Histograms of total homogenization temperatures (Th, tot) to liquid (B) or vapor (C) of type II inclusions.

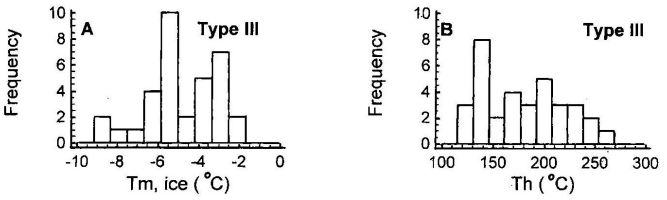


**Fig. 9. A.** Histogram of final ice melting temperatures Tm, ice in type III inclusions. **B.** Histogram of temperatures of homogenization (to liquid) of type III inclusions.

inclusions (HEDENQUIST and HENLEY, 1985). Type III inclusions homogenized to the liquid phase at temperatures between 130° and 269 °C (Fig. 9B). Densities of type III inclusions range between 0.84 and 0.92 g/cc, and were calculated in the system $H_2O$-NaCl with the use of the EOS by ZHANG and FRANTZ (1987).

## Discussion

The presence of decrepitated type IV inclusions indicates that following entrapment, the internal pressure of the inclusion exceeded the confining pressure plus the cohesion of the host quartz by an amount sufficient to rupture the inclusion (e.g. VITYK and BODNAR, 1995; VITYK et al. 1995; 1996). In addition, leaked inclusions may be interpreted as the result of re-equilibration to a lower bulk density under conditions of high internal overpressures (e.g. GILES and MARSHALL, 1994; VITYK and BODNAR, 1995; VITYK et al. 1995; 1996, MARSHALL et al., 2000). The latter interpretation may apply to one-phase inclusions, assigned to type III, in the vicinity of decrepitated inclusions, or alternatively, these inclusions are the result of metastability due to their small size (~4 μm). High internal overpressures and decrepitation, and/or leakage, within inclusions are consistent with the host vein-quartz crystals undergoing a major late syn- to post-depositional decompression event as a response to reduction of confining pressures. This is commonly the result of uplift and concurrent exhumation in a tectonic extensional environment (e.g. CRAW, 1988; GILES and MARSHALL, 1994; BAKKER and MAMTANI, 2000; MARSHALL et al., 2000). Uplift from mid-crustal depths is also supported by deformation microstructures in quartz which indicate that the vein was forced through the ductile-brittle transition resulting in the overprinting of ductile strain textures by brittle fractures (Fig. 4). Also, tectonic extension may be considered as the mechanism of brittle failure of the quartz generating the abundant healed microfractures occupied by type III aqueous inclusions.

Calculated type II inclusion isochores are spread and show a wide range of apparent conditions of entrapment with relatively $H_2O$-rich inclusions projecting to higher pressures, and relatively carbonic rich inclusions at lower pressures (Fig. 10). Isochores for type I inclusions were calculated using the EOS according to DUAN et al. (1992a, b) for pure $CO_2$. The EOS according to BOWERS and HELGESON (1983), adopted by BAKKER (1999 b) to include $CH_4$ and $N_2$, coupled by microthermometry data and visual estimation of volume fractions of the fluid phases, were used to calculate the isochores for type II inclusions (program package FLUIDS). Also, isochores of type I and II inclusions were calculated including the thermal expansion and compressibility of the host mineral quartz according to HOSIENI et al. (1985) (see BAKKER and MAMTANI, 2000). Isochore distribution is difficult to interpret as the result of alternate trapping of very distinct fluid types. Calculated isochore for a selected isolated $H_2O$-rich (90 vol.% $H_2O$) type II inclusion

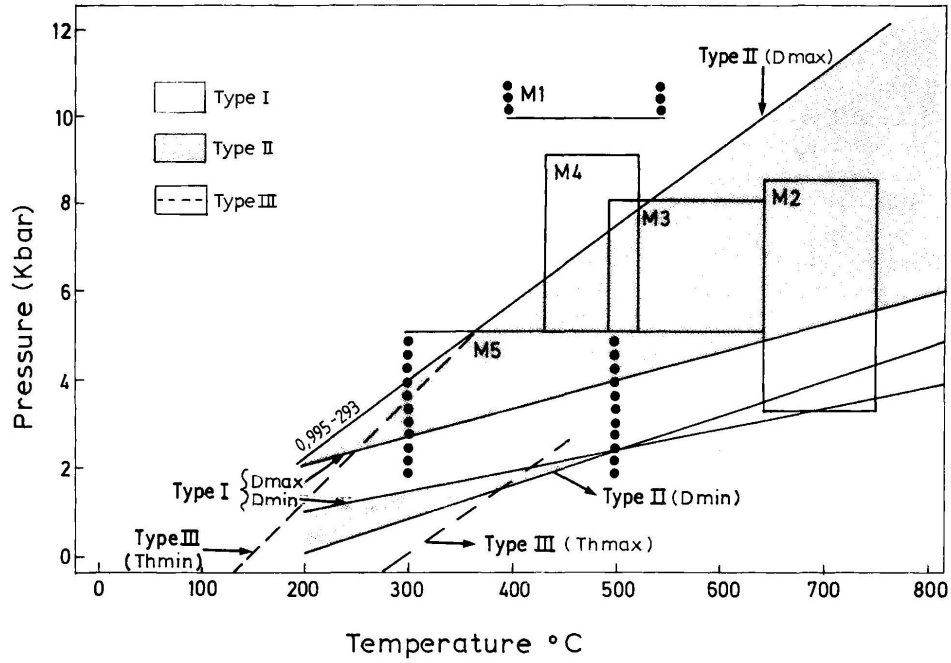


**Fig. 10.** Pressure-temperature diagram showing calculated calculated isochores for type I, II and III inclusions, in relation to inferred regional metamorphic conditions in the NW Vertiskos Formation. Sources of data KOUROU (1991) and SIDIROPOULOS (1991) (see text for discussion).

with the highest density found and high $T_h$ (d = 0.9953 g/cc, Th: 293 °C), and showing the highest P-T conditions amongst the measured inclusions, crosses the inferred $M_4$ metamorphic P-T conditions at T: 440–520 and P: 6–8 kbar (Fig. 10). Isochores for other type II inclusions with lower density, and the isochores of type I inclusions, pass through lower pressure conditions, spanning the P-T range through the waning stages of $M_4$ and the P-T range of $M_5$. Considering that the lack of biotite, or high P-T assemblages, may impose an upper temperature limit of 450 °C for the formation of vein quartz, the above relationships may suggest that the fluid in isolated type II inclusions with the highest density may represent relics of the original $M_4$ metamorphic fluid, and early deposition of vein quartz may have commenced at $M_4$ conditions (maximum P of ~6 kbar at maximum T~450 °C). Furthermore, the isochore distribution may be interpreted as entrapment of an evolving fluid during decompressive uplift and changes in structural levels (CATHELINEAU, et al. 1993; BAKKER and MAMTANI, 2000), fluctuating pressure conditions (ROBERT and KELLY, 1987), or immiscibility and heterogeneous trapping (see below) (RAMBOZ et al., 1982). It should be emphasized that the inferred decompression, and hence uplift, path is constrained to follow the isochores of type II inclusions, and at the same time lie no further than 2 kbar below the isochore for the densest inclusion. The latter constraint is imposed by the assumption that >2 kbar difference in pressure between the high-density inclusions and ambient conditions could cause re-equilibration of early inclusions depending on their size (BAKKER and JANSEN, 1990; 1994; VITYK and BODNAR, 1995). The scatter in inclusion isochores to >3 kbar below the isochore for the densest inclusion

may suggest inclusion re-equilibration under conditions of >3 kbar internal overpressure, or alternatively may be interpreted as a result of errors in the calculations from visual estimation of phase proportions, or local fluid immiscibility accompanied by heterogeneous fluid trapping (see below).

An alternative interpretation is that coexisting inclusion types I and II may represent the products of phase separation (unmixing) of an initial $H_2O$–$CO_2$ parent fluid, prior to, or during entrapment, due to decompression (RAMBOZ et al., 1982). Regional uplift may initiate fluid unmixing by forcing a deep hydrothermal fluid flow regime through the solvus of the respective chemical system in response to the uplift-induced gradual pressure reduction (CRAW, 1992; RUSHTON et al., 1993). The unmixing process may have resulted in the complex trapping of two immiscible fluids: a $CO_2$-rich end member, represented by type I inclusions (considering an undetected content of ~10 vol.% $H_2O$) and a $H_2O$-rich end-member, represented by type II inclusions with the lowest volumetric percentage of carbonic phase (< = 10 vol. %) and the highest density. This interpretation may be supported by type II inclusions with low volumetric percentage of carbonic vapor phase which homogenize to the aqueous phase and type I inclusions in the same sample, and, $H_2O$-rich and $CO_2$-rich type II inclusions which homogenize at the same temperature range, into the aqueous or carbonic phase, respectively (Fig. 8B, C). However, the latter interpretation should be considered with caution, because the Th data distribution (Fig. 8B, C) shows a rather flattened, and hence difficult to interpret, pattern. If inclusion types I and II are the products of immiscibility, minimum Th conditions of 200–250 °C (Fig. 8B, C) at calculated Ph between 0.25 and 1.8 kbar may be considered as conditions of fluid unmixing and fluid inclusion trapping. Pressure at homogenization for type II inclusions was calculated with the aid of computer program GASWET (BAKKER, 1999b) using the EOS by BOWERS and HELGESON (1983) for the in the system $H_2O$–$CO_2$–NaCl adopted by BAKKER (1999b) to include $CH_4$ and $N_2$. If type II inclusions are truly related to vein filling, and constitute products of immiscibility, then the above fluid unmixing P-T conditions may represent depositional conditions of the majority of the vein quartz.

On the basis of similar mode of occurrence with decrepitated and/or leaked inclusions, and wide range in calculated isochores, it may be suggested that type I and II inclusion may have also been trapped under conditions of internal overpressure. Consequently, the validity of the above microthermometry data interpretation rely basically on the question whether measured regularly shaped inclusions have maintained their original density. Laboratory experiments (VITYK and BODNAR, 1995; 1998; VITYK et al., 2000) have shown that a large number of the relatively smaller synthetic aqueous saline fluid inclusions in quartz may maintain original densities and homogenization temperatures during cooling and decompression, after having experienced internal overpressures up to 2 kbar in excess of confining pressure. Experimental data on synthetic $H_2O$–$CO_2$ fluid inclusions have shown that isothermal decompression at supercritical conditions may cause non-decrepitative preferential loss of $H_2O$ through microfractures and dislocations, and density resetting to lower values (BAKKER and JANSEN, 1990;1994); in the latter case textures indicative of these modifications were not evident. Recent studies of natural fluid inclusions in medium and high grade metamorphic rocks and high-T lode gold deposits (RIDLEY and HAGEMANN, 1999; BAKKER and MAMTANI, 2000) have shown that in order to critically evaluate fluid inclusion data for post entrapment modifications, it is necessary that the fluid inclusion record is compared against independent constraints on P-T-X conditions obtained from mineral equilibria. BAKKER and MAMTANI (2000) identified

relics of original peak metamorphic fluids in quartz from a lower amphibolite-facies biotite-garnet schist from India, in the form of isolated carbonic inclusions. This was achieved by comparing fluid inclusion calculated isochores with calculated P-T conditions from garnet geothermobarometry. These authors have also identified inclusions which were subjected to post-entrapment inclusion re-equilibration processes (i.e. preferential leakage of $H_2O$ and partial decrepitation) as a result of post-metamorphic decompression and uplift; however, they have suggested that the relatively smaller early formed inclusions (2–4 μm) can resist high overpressures and remain conserved during decompression. RIDLEY and HAGEMANN (1999), in a study of Australian high-T lode gold deposits, found aqueous-carbonic fluid inclusions with a wide range of compositions and densities. Calculated inclusion isochores yielded fluid entrapment pressures deviating by ± 2 kbar from independent estimates based on petrologic equilibria. They suggested that post-entrapment inclusion re-equilibration (i.e. diffusional addition of $H_2$ into inclusions, diffusional loss of $H_2O$, reduction of inclusion volume) is to be suspected as the cause of these inconsistencies. However, preliminary work from other Australian deposits revealed similar inclusions shown to be largely unaffected by post-entrapment modification despite high entrapment temperatures of ~600 °C (see RIDLEY and HAGEMANN, 1999). The above studies have also shown that inclusion re-equilibration and modification processes, do not take place uniformly within single crystals (BAKKER and MAMTANI, 2000), and are not uniformly developed within a vein system and within individual clusters of inclusions (RIDLEY and HAGEMANN, 1999). The above discussion suggests that even if type I and II inclusions in this study have maintained their original densities during post-entrapment decompression, the validity of the calculated results can not be tested due to the lack of independent means of P-T estimation of the conditions of vein formation.

Type III inclusions with lower Th than those of the aqueous-carbonic inclusions (8B, C; 9B), and low modal salinity (5.4 wt% NaCl equiv.), are consistent with a late hydrothermal event (e.g. GILES and MARSHALL, 1994, RUSHTON et al., 1993, RIDLEY and HAGEMANN, 1999; MARSHALL et al., 2000). Decompression of the vein accompanying uplift may be considered as the mechanism of brittle failure of the quartz generating the abundant healed microfractures occupied by type III aqueous inclusions. Type III inclusions clearly overprint all other fluid inclusion populations, as well as any microscale evidence of ductile deformation, cataclasis and recrystallization. Consequently, they were trapped subsequent to the decrepitation event and quartz ductile deformations, recrystallization and recovery. Such inclusions are interpreted as a record of the influx of high-level meteoric fluids late within an ongoing tectonic extensional regime, and are related to microfractures formed along the uplift path in the brittle regime above the brittle/ductile transition (GILES and MARSHALL, 1994; RUSHTON et al., 1993; NESBITT and MUELENBACHS, 1995; MARSHALL et al., 2000). Uplift almost inevitably leads to the growth of steep topographic gradients, thus creating a hydraulic head which can drive meteoric waters downward into the crust (CHAMBERLAIN et al., 1995). The minor occurrence of $CO_2$ in some type III inclusions may be explained by mixing of meteoric water with trapped aqueous(?)-carbonic fluids released during decompression (GILES and MARSHALL, 1994). Isochore distribution for type III inclusions which span a wide range of apparent trapping conditions support decompression as the cause of brittle failure in quartz and trapping of type III inclusions (Fig. 10). Isochores were calculated with the use of the EOS by ZHANG and FRANTZ (1987) in the system $H_2O$-NaCl. When aqueous fluid

inclusions are trapped in such an environment, original trapping conditions may be approximated by the isochore corresponding to the minimum Th value (130 °C), whereas the maximum Th value (269 °C) approximates the Th of the isochore representing final re-equilibration or trapping conditions (VITYK and BODNAR, 1998). The P-T path followed by type III inclusions after and/or during entrapment would be constrained to lie below the 130 °C and above the 269 °C isochore (Fig. 10). Figure 10 suggests that internal overpressure for type III inclusions with the highest density (130 °C) corresponds to >3 kbar. Consequently, it is unlikely that type III inclusions with minimum Th represent original densities and conditions. Inclusions with the highest Th (~270 °C) could be original inclusions that were re-equilibrated or, they could represent new inclusions trapped either during incremental decompression or at the final P-T conditions during continued fracture healing (VITYK and BODNAR, 1998). If this is the case here, the late hydrothermal event represented by type III inclusions may have taken place at low pressures (<1 kbar) and maximum T ~270 °C during continuing decompression and uplift (Fig. 10).

## Concluding remarks

Quartz from the Kastri vein-quartz deposit is characterized by syn-depositional ductile strain (quartz 1), local cataclasis and recrystallization (quartz 2), and superimposed brittle fracturing. Vein quartz has numerous fluid inclusions in different configurations, as isolated inclusions or groups, in trails, and along (sub-)grain boundaries. Five types of fluid inclusions (I–IV) are recognized: Type I, carbonic $CO_2$ ($\pm H_2O$) inclusions, type II, low salinity (0.9–14.4 wt% eq. NaCl) aqueous-carbonic $H_2O$–$CO_2$–NaCl ($\pm CH_4$–$N_2$) inclusions with highly variable aqueous:carbonic phase ratios, and decrepitated/leaked type IV inclusions, occur as isolated inclusions or groups within quartz 1 grains, and are interpreted as most likely related to vein filling. Type III, aqueous $H_2O$–NaCl ($\pm CO_2$) inclusions occur mainly in trails crosscutting both quartz 1 and 2, and are interpreted as post vein filling hydrothermal fluids, whereas type V inclusions are extremely late and occur along quartz 2 grain boundaries.

Natural decrepitation and leakage textures of type IV inclusions may be attributed to syn- or post-entrapment decompression causing internal overpressures within the inclusions, accompanying extension, decompressive uplift and concurrent exhumation of VF. Uplift from mid-crustal depths is also supported by deformation microstructures in quartz which indicate that the vein was forced through the ductile/brittle transition resulting in the overprinting of ductile strain textures by brittle fractures. The decrepitation and leakage event may have resulted in re-equilibration of early formed low salinity apparently metamorphic aqueous-carbonic fluids giving rise to the present configuration of inclusion types I and II. This is supported by the wide range in compositions, and, calculated densities and isochores of type I and II inclusions which suggest an unreasonably wide range of fluid pressures during formation of the deposit. However, in the absence of independent constraints on the P-T-X conditions of vein formation the possibility of post-entrapment reequilibration of inclusion types I and II cannot be critically evaluated.

If the variability in fluid inclusion P-V-T-X properties is not a result of inclusion re-equilibration, then type I and II fluid inclusions may be interpreted either as records of an evolving fluid during decompression and uplift , or products of fluid unmixing triggered by uplift and confining pressure reduction. In the first case the higher density type II

inclusions may represent relics of the original $M_4$ metamorphic fluid, and the lower density type II, and type I, inclusions may have trapped a fluid evolving in parallel with the waning stages and retrogression of the $M_4$ metamorphic event to $M_3$ conditions. Consequently, vein filling may have started at $M_4$ metamorphic conditions (maximum P-T conditions of ~6 kbar and 450 °C), and continued down to $M_5$ conditions during syn- to post-metamorphic uplift. In the second case, vein filling conditions are constrained by the conditions of fluid unmixing at post-metamorphic conditions between 200–250 °C and pressures 0.25–1.8 kbar, during ongoing decompressive uplift. Whether inclusion types I and II represent fluid inclusion re-equilibration products, syn-metamorphic fluid evolution during decompressive uplift or syn- to post-metamorphic immiscibility processes induced by decompression, or a combination of the above, cannot be verified only with the present data.

Decompression of the vein accompanying uplift may be considered as the mechanism of brittle failure of the quartz generating the abundant healed microfractures occupied by type III aqueous inclusions. Given their late nature and apparent conditions of entrapment, type III inclusions with the highest $T_h$ may possibly record trapping conditions of deeply circulating meteoric water into brittle fractures during ongoing decompression late in the uplift history. Regional uplift of VF may be related to the Late Cenozoic evolution of the region characterized by extensional tectonics.

## Acknowledgements

This research is part of a BRITE-EURAM II Project entitled "New industrial applications for quartz deposits indigenous to the Community"(BE-8226). Financial support provided by the EU is gratefully acknowledged.

Drs. R. BAKKER and V. LUDERS are thanked for two constructive reviews that greatly improved the final version of the manuscript.

## References

ARVANITIDIS, N.D.: New industrial applications for quartz deposits indigenous to the Community. In: KONTOPOULOS, A., PASPALIARIS, I., ADJEMIAN, A., and KATALAGARIANAKIS, G. (eds.) "European Thematic Network on Extractive Industries-Proceedings of the first annual workshop (EUROTHEN '98)", National Technical University of Athens (1998), 559–568.

ARVANITIDIS, N.D., and KILIAS, S.P.: Vein-quartz deposits of northern Greece-Exploitable resources for industrial uses. In: Papunen, H. (ed.) Mineral Deposits: Research and Exploration Where do they meet? Balkema (1997), 701–704.

BAKKER, R.J.: CLATHRATES: computer programs to calculate fluid inclusion V–X properties using clathrate melting temperatures. Computers & Geosciences **23** (1997), 1–18.

BAKKER, R.J.: Optimal interpretation of microthermometrical data from fluid inclusions: thermodynamic modelling and computer programming. Habilitation thesis, Univ. Heidelberg, Germany (1999a).

BAKKER, R.J.: Adaptation of the Bowers and Helgeson (1983) equation of state to the $H_2O$–$CO_2$–$CH_4$–$N_2$–NaCl system. Chemical Geology **154** (1999b), 225–236.

BAKKER, R.J., and JANSEN, J.B.H.: Preferential water leakage from fluid inclusions by means of mobile dislocations. Nature **345** (1990), 58–60.

BAKKER, R.J., and JANSEN, J.B.H.: A mechanism for preferential $H_2O$ leakage from fluid inclusions in quartz, based on TEM observations. Contrib. Mineral. Petrol. **116** (1994), 7–20.

BAKKER, R.J., DUBESSY, J., and CATHELINEAU, M.: Improvements in clathrate modelling: The $H_2O$–$CO_2$ system with various salts. Geochim. Cosmochim. Acta **60** (1996), 1657–1681.

BAKKER, R.J., and MAMTANI, M.A.: Fluid inclusions as metamorphic process indicators in the Southern Aravalli Mountain Belt (India). Contrib. Mineral. Petrol. **139** (2000), 163–179.

BODNAR, R.J.: Revised equation and table for determining the freezing point depression of $H_2O$–NaCl solutions. Geochim. Cosmochim. Acta **57** (1993), 683–684.

BORISENKO, A. S.: Study of the salt composition of solutions in gas-liquid inclusions in mineral by the cryometric method. Soviet. Geol. and Geophys. **18** (1977), 11–19.

BOWERS, S., and HELGESON, H.C.: Calculation of the thermodynamic and geochemical consequences of non ideal mixing in the system $H_2O$-$CO_2$-NaCl on phase relations in geologic systems: Equation of state for $H_2O$-$CO_2$-NaCl fluids at high pressures and temperatures. Geochim. Cosmochim. Acta **47** (1983), 1247–1275.

CATHELINEAU, M., BOIRON, M.C., ESSARRAJ, S., DUBESSY, J., LESPINASSE, M., and POTY, B.: Fluid pressure variations in relation to multistage deformation and uplift : a fluid inclusion study of Au quartz veins. Eur. J. Mineral. **5** (1993),107–121.

CHAMBERLAIN, C.P., ZEITLER, P.K., BARNETT, D.E., WINSLOW, D., POULSON, S.R., LEAHY, T., and HAMMER, J.E.: Active hydrothermal systems during the recent uplift of Nanga Parbat, Pakistan Himalaya. Journal of Geophysical Research **100** (1995), 439–453.

CHRISTOFIDES, G., D' AMICO, C., DEL MORO, A., ELEFTHERIADIS, G., and KYRIAKOPOULOS, C.: Rb/Sr geochronology and geochemical characters of the Sithonia plutonic complex (Greece). Eur. J. Mineral. **2** (1990), 79–87.

CRAW, D.: Shallow-level metamorphic fluids in a high uplift rate metamorphic belt; Alpine schist, New Zealand. J. Metamorphic Geol. **6** (1988), 1–16.

CRAW, D.: Fluid evolution fluid immiscibility and gold deposition during Cretaceous-Recent tectonics and uplift of the Otago and Alpine Schist, New Zealand. Chem. Geol. **98** (1992), 221–236.

DE WET, A. P., MILLER, J.A., BICKLE, M.J., and CHAPMAN, H.J.: Geology and geochronology of the Arnea, Sithonia and Ouranoupolis, intrusions, Chalkidiki Peninsula, northern Greece. Tectonophysics **161** (1989), 65–79.

DIAMOND, L.W.: Fluid inclusion evidence for P-V-T-X evolution of hydrothermal solutions in late-Alpine gold quartz veins at Brusson, Val D'Ayas, NW Italian Alps. Am. J. Sci. **290** (1990), 912–958.

DIAMOND, L.W.: Stability of $CO_2$ clathrate hydrate +$CO_2$ liquid +$CO_2$ vapor + aqueous KCl-NaCl solution: experimental determination and applications to salinity estimates of fluid inclusions. Geochim. Cosmochim. Acta **56** (1992), 273–280.

DARLING, R.S.: An extended equation to calculate NaCl contents from final clathrate melting temperatures in $H_2O$-$CO_2$-NaCl fluid inclusions: implications for P-T isochore location. Geochim. Cosmochim. Acta **55** (1991), 3869–3871.

DIMITRIADIS, S. and GODELITSAS, A.: Evidence for high pressure metamorphism in the Vertiskos group of the Servomacedonian massif: the eclogite of Nea Roda. Bull. Geol. Soc. Greece **25/2** (1991), 67–80.

DINTER, D.A.: Late Cenozoic extension of the Alpine collisional orogen, northeastern Greece: Origin of the north Aegean basin. GSA Bulletin **110** (1998), 1208–1230.

DINTER, D.A., and ROYDEN, L.: Late Cenozoic extension in northeastern Greece: Strymon Valley detachment and Rhodope metamorphic core complex. Geology **21** (1993), 45–48.

DUAN, Z., MOLLER, N. and WEARE, J.H.: An equation of state for the $CH_4$–$CO_2$–$H_2O$ system: I. Pure systems from 0 to 1000 °C and 0 to 8000 bar. Geochim. Cosmochim. Acta **56** (1992a), 2605–2617.

DUAN, Z., MOLLER, N. and WEARE, J.H.: An equation of state for the $CH_4$–$CO_2$–$H_2O$ system: II. Mixtures from 50 to 1000 °C and 0 to 1000 bar. Geochim. Cosmochim. Acta **56** (1992b), 2619–2631.

DUSCHEK, W., KLEINRAHM, R., and WAGNER, W.: Measurement and correlation of the (pressure, density, temperature) relation of carbon dioxide II. Saturated-liquid and saturated-vapour densities and the vapour pressure along the entire coexistence curve. J. Chem. Thermodynamics **22** (1990), 841–864.

ECHTLER, H., MATTE, P., and MALUSKI H.: Large southwestward ductile thrusting in the alpine Serbo-Macedonian belt. (abstract) Terra Cognita **248** (1987), 106.

FREI, R.: Isotope (Pb, Rb-Sr, S, O, C, U-Pb) geochemical investigations on Tertiary intrusives and related mineralizations in the Servomacedonian Pb–Zn, Sb+Cu–Mo metallogenetic province in Northern Greece. Unpubl. Ph.D. thesis, ETH Zurich (1992).

GILES, A.D., and MARSHALL, B.: Fluid inclusion studies on a multiply deformed, metamorphosed volcanic associated massive sulfide deposit, Joma mine, Norway. Econ. Geol. **89** (1994), 803–819.

HARRE, W., KOCKEL, F., KREUZER, H., LENZ, H., MULLER, P., and WALTHER, H.W.: Uber Rejuvenationen im Serbo-Madzedonischen Massiv (Deutung radiometrischer Altersbestimmungen). Proc. International Geological Congress 23rd, Prague **6** (1968), 223–236.

HENDEQUIST, J.W., and HENLEY, R.W.: The importance of $CO_2$ freezing point measurements of fluid inclusions: Evidence for geothermal systems and implications for epithermal ore deposition. Econ. Geol. **80** (1985), 1379–1406.

HOSIENI, K.R., HOWALD, R.A., and SCANLON M.W.: Thermodynamics of the lambda transition and the equation of state of quartz. Am. Mineral. **70** (1985), 782–793.

KAUFMANN, G., KOCKEL, F., and MOLLAT, H.: Notes on the stratigraphic and paleographic position of the Svoula Formation in the innermost zone of the Hellenides (N. Greece). Bull. Soc. Geol. France (VII) **18** (1976), 225–230.

KOCKEL, F. H., MOLLAT, H., and WALTHER, H.W.: Erlanterungen zur geologischen Karte den Chalkidiki und angrenzender Gebiete 1:100000 Nordgriechenland. Bundesamt. Geowiss. Rohst., Hannover, (1977)

KOUGOULIS, C., VERANIS, N., and KASSOLI-FOURNARAKI, A.: Metavolcanic rocks in the Examili Formation (North Greece). Chem. Erde **50** (1990), 67–79.

KOUROU, A.: Lithology, tectonics, geochemistry and metamorphism of part of western Vertiskos Group. The northeastern area of the Agios Vassilios Lake (Koronia). Unpubl. Ph.D. thesis, Univ. Thessaloniki, 575 p. (in Greek with English abstract) (1991)

LEE, B.I., and KESLER, M.G.: A generalized thermodynamic correlation based on three-parameter corresponding states. Am. Inst. Chemical Engineering Jour. **21** (1975), 510–527.

MARSHALL, B., GILES, A.D., and HAGEMANN, S.G.: Fluid inclusions in metamorphosed and synmetamorphic (including metamorphogenic) base and precious metal deposits: indicators of ore-forming conditions and/or ore-modifying histories? Reviews in Economic Geology **11** (2000), 119–148.

MOUNTRAKIS, D.: Introduction to the Geology of Macedonia and Thrace. Aspects of the geotectonic evolution of the Hellenic Hinterland and Internal Hellenides. Bull. Geol. Soc. Greece **30** (1994), 31–46. (in Greek with English abstract)

NESBITT, B.E., and MUEHLENBACHS, K.: Geochemical studies of the origins and effects of synorogenic fluids in the southern Omineca crystalline belt of British Columbia, Canada. Geological Society of America Bulletin **107** (1995), 1033–1050.

PATRAS, D., KILIAS, A., CHADZIDIMITRIADIS, E., and MUNTRAKIS, D.: Study of the formation phases of the internal Hellenides in northern Greece. Bull. Geol. Soc. Greece **20** (1986), 139–157 (in Greek with English abstract).

RAMBOZ, C., PICHAVANT, M., and WEISBROD, A.: Fluid immiscibility in natural processes: use and misuse of fluid inclusion data in terms of immiscibility. Chem. Geol. **37** (1982), 29–48.

RIDLEY, J., and HAGEMANN, S.G.: Interpretation of post-entrapment fluid inclusion re-equilibration at the Three Mile Hill, Marvel Loch and Griffins Find high-temperature lode-gold deposits, Yilgarn Craton, Western Australia. Chemical Geology **154** (1999), 257–278.

ROBERT, F., and KELLY, W.C.: Ore-forming fluids in Archean gold-bearing quartz veins at the Sigma mine, Abitibi greenstone belt. Econ. Geol. **82** (1987), 1464–1482.

RUSHTON, R.W., NESBITT, B.E., MUEHLENBACHS, K., and MORTENSEN, J.K.: A fluid inclusion and stable isotope study of Au quartz veins in the Klondike district, Yukon Territory, Canada: A section through a mesothermal vein system. Econ. Geol. **88** (1993), 647–678.

SAKELLARIOU, D.: Geologie des Serbomazedonischen Massivs in der nordostlichen Chalkidiki, N. Griechenland-Deformation und Metamorphose. Unpubl. Ph.D. thesis, Univ. Mainz (1989)

SHEPHERD, T.J., RANKIN, A.H., and ALDERTON, D.H.M.: A practical guide to fluid inclusions studies. Blackie & Sons, Glasgow (1985)

SIDIROPOULOS, N.: Lithology, geochemistry, tectonics and metamorphism of the northwestern part of the Vertiskos Group. The mountain Disoron (Krousia) area, north of Kilkis. Unpubl. Ph.D. thesis, Univ. Thessaloniki, (1991) (in Greek with English abstract)

SPAN, R., and WAGNER, W.: A new equation of state for carbon dioxide covering the fluid region from the triple point temperature to 1100 K at pressures up to 800 MPa. J. Phys. Chem. Ref. Data **25** (1996), 1509–1596.

STERNER, S.M., and BODNAR. R.: Synthetic fluid inclusions-VII. Re-equilibration of fluid inclusions in quartz during laboratory – Simulated metamorphic burial and uplift. J. Metamorphic Geol. **7** (1989), 243–260.

THIERY, R., VAN DEN KERKHOF, A.M., and DUBESSY, J.: vX properties of $CH_4$–$CO_2$ and $CO_2$–$N_2$ fluid inclusions: modelling for $T < 31$ °C and $P < 400$ bars. Eur. J. Mineral. **6** (1994), 753–771.

VERANIS, N., KOUGOULIS, C., and KASSOLI-FOURNARAKI, A.: The Examili Formation and its relations to the Vertiskos subzone of the Serbo-Macedonian massif. Bull. Geol. Soc. Greece **22** (1990), 71–86.

VITAL, C.: Mineralogical and petrographical investigations of the area between Arnea and Megali Panagia, Chalkidiki Peninsula (N. Greece). Unpubl. B.Sc. thesis, ETH Zurich (1986)

VITYK, M.O., and BODNAR, R.J.: Do fluid inclusions in high-grade metamorphic terranes preserve peak metamorphic density during retrograde decompression? American Mineralogist **80** (1995), 641–644.

VITYK, M.O., BODNAR, R. J., and DUDOK I.V: Natural and synthetic re-equilibration textures of fluid inclusions in quartz (Marmarosh Diamonds): Evidence for refilling under conditions of compressive loading. Eur. J. Mineral. **7** (1995), 1071–1087.